Molecular Motions and Protein Folding: Characterization of the Backbone Dynamics and Folding Equilibrium of α_2D Using ^{13}C NMR Spin Relaxation

R. Blake Hill,[†] Clay Bracken,[‡] William F. DeGrado,*,[†] and Arthur G. Palmer III*,[§]

Contribution from the Johnson Research Foundation, Department of Biochemistry and Biophysics, University of Pennsylvania, Philadelphia, Pennsylvania 19104-6059, Department of Biochemistry, Weill Medical College of Cornell University, New York, New York 10021, and Department of Biochemistry and Molecular Biophysics, Columbia University, New York, New York 10032

Received March 30, 2000. Revised Manuscript Received October 2, 2000

Abstract: De novo protein design enables systematic exploration of the relationship between the amino acid sequences, conformations, and thermodynamics of proteins. The polypeptide α_2D is a de novo designed dimeric four-helix bundle with a native-like three-dimensional structure [Hill, R. B.; DeGrado, W. F. *J. Am. Chem. Soc.* **1998**, *120*, 1138−1145]. The roles of intramolecular conformational dynamics and folding kinetics in determining the equilibrium properties of α_2D have been investigated using novel NMR spin relaxation methods. To facilitate these experiments, the four leucine residues in the α_2D monomer were labeled specifically with ^{13}C at the C$^{\alpha}$ position. Reduced spectral densities [Farrow, N. A.; Zhang, O.; Szabo, A.; Torchia, D. A.; Kay, L. E. *J. Biomol. NMR* **1995**, *6*, 153−162] were obtained from spin relaxation data recorded at four static magnetic fields and were interpreted using the model-free formalism [Lipari, G.; Szabo, A. *J. Am. Chem. Soc.* **1982**, *104*, 4546−4559]. Generally, the backbone mobility of α_2D is typical of natural proteins. High C$^{\alpha}$ order parameters indicate that motions are restricted on the picosecond to nanosecond time scale. Slightly lower order parameters and longer internal correlation times are observed for the most N-terminal and C-terminal sites. Chemical exchange linebroadening is manifest for all leucine ^{13}C$^{\alpha}$ spins and results from the folding equilibrium of α_2D. The chemical exchange process was characterized using the relaxation-compensated Carr−Purcell−Meiboom−Gill experiment [Loria, J. P.; Rance, M.; Palmer, A. G., III. *J. Am. Chem. Soc.* **1999**, *121*, 2331−2332]. The folding and unfolding rate constants were measured to be $(4.7 \pm 0.9) \times 10^6$ M^{-1} s^{-1} and 15 ± 3 s^{-1}, respectively, and agree with the equilibrium constant for folding of α_2D. The ^{13}C$^{\alpha}$ chemical shifts for unfolded and folded forms of α_2D, obtained from this analysis, indicate that the ensemble of unfolded states includes transiently structured helical conformations. The results both confirm the success of the de novo design strategy and suggest avenues for further improvement of the native-like properties of α_2D.

De novo protein design provides a powerful approach for testing the principles governing the structural, dynamic, and functional properties of proteins.[1] Several groups have used this approach to probe the features required for folding a polypeptide into a well-defined conformation that includes an efficiently packed hydrophobic core.[2] Initial attempts to design proteins generally led to structures with dynamically averaged conformations, similar to the molten globule states of proteins.[3] More recently, considerable success has been demonstrated in the design of coiled coils,[4−12] three-stranded antiparallel β-sheets,[13,14] and zinc finger motifs.[15,16] These peptides fold into the desired native-like three-dimensional structures, although they show marginal thermodynamic stabilities. The design of larger proteins with unique conformations has proven to be more difficult. Mayo and co-workers designed a tetrameric β-protein based on the sequence of Interleukin-4.[17] Structural studies demonstrated that the protein was composed of a dimer with two conforma-

---

* Address correspondence to W.F.D. (E-mail, degrado@mail.med.upenn.edu; telephone, (215) 898-4590; fax, (215) 573-7229) or A.G.P. (E-mail, agp6@columbia.edu; telephone, (212) 305-8675; fax, (212) 305-6949).

[†] University of Pennsylvania.

[‡] Cornell University.

[§] Columbia University.

(1) Bryson, J. W.; Betz, S. F.; Lu, H. S.; Suich, D. J.; Zhou, H. X.; O'Neil, K. T.; DeGrado, W. F. *Science* **1995**, *270*, 935−941.

(2) DeGrado, W. F.; Summa, C. M.; Pavone, V.; Nastri, F.; Lombardi, A. *Annu. Rev. Biochem.* **1999**, *68*, 779−819.

(3) Betz, S. F.; Raleigh, D. P.; DeGrado, W. F. *Curr. Opin. Struct. Biol.* **1993**, *3*, 601−610.

(4) Ghirlanda, G.; Lear, J. D.; Lombardi, A.; DeGrado, W. F. *J. Mol. Biol.* **1998**, *281*, 379−391.

(5) Gernert, K. M.; Surles, M. C.; Labean, T. H.; Richardson, J. S.; Richardson, D. C. *Protein Sci.* **1995**, *4*, 2252−2260.

(6) Gonzalez, L., Jr.; Plecs, J. J.; Alber, T. *Nat. Struct. Biol.* **1996**, *3*, 510−515.

(7) Gonzalez, L., Jr.; Woolfson, D. N.; Alber, T. *Nat. Struct. Biol.* **1996**, *3*, 1011−1018.

(8) Lombardi, A.; Bryson, J. W.; DeGrado, W. F. *Biopolymers* **1996**, *40*, 495−504.

(9) Lumb, K. J.; Kim, P. S. *Science* **1996**, *271*, 1137−1138.

(10) O'Shea, E. K.; Lumb, K. H.; Kim, P. S. *Curr. Biol.* **1993**, *3*, 658−667.

(11) Oakley, M.; Kim, P. *Biochemistry* **1998**, *37*, 12603−12610.

(12) Schneider, J. P.; Lombardi, A.; DeGrado, W. F. *Folding Des.* **1998**, *3*, R29−R40.

(13) Kortemme, T.; Ramirez-Alvarado, M.; Serrano, L. *Science* **1998**, *281*, 253−256.

(14) Schenck, H. L.; Gellman, S. H. *J. Am. Chem. Soc.* **1998**, *120*, 4869−4870.

(15) Struthers, M. D.; Cheng, R. P.; Imperiali, B. *Science* **1996**, *271*, 342−345.

(16) Dahiyat, B. I.; Mayo, S. L. *Science* **1997**, *278*, 82−87.

(17) Mayo, K. H.; Ilyina, E.; Park, H. *Protein Sci.* **1996**, *5*, 1301−1315.

10.1021/ja001129b CCC: $19.00

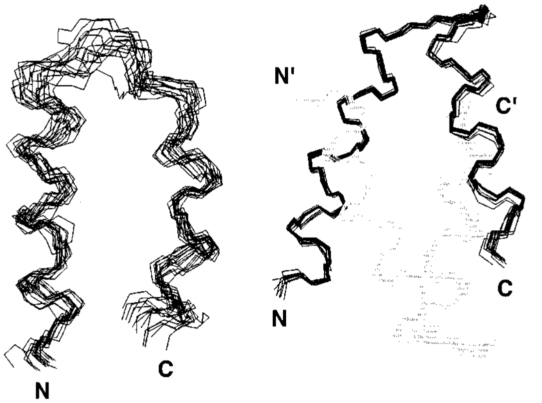

Figure 1. Structural comparison between α-t-α and α_2D. Superposition of the C^α backbone from the 16 lowest energy NMR structures for (left) α-t-α and (right) α_2D. The figure was drawn from the coordinates of PDB files 1abz (α-t-α) and 1qp6 (α_2D) using InsightII (MSI Research).

tions that were in slow exchange on the millisecond time scale; these dimers further associated in a nonspecific manner about a hydrophobically stabilized interface that lacked a well-defined conformation.[18] Similarly, a tetrameric α-helical peptide was shown to adopt a conformationally mobile dimer of partially structured dimers.[19] Finally, the crystal structure of a four-helix bundle with four identical helices connected by three glycine-rich loops was found to have statistically disordered loops.[20] Whether this protein was a left-handed or a right-handed bundle, or a mixture of these two topologies, could not be determined. Despite these obstacles, the solution structures of several uniquely folded proteins have been determined, including two-, three-, and four-helix bundles.[21−23]

Comprehensive assessment of the success of a de novo design strategy requires knowledge of the structures, thermodynamics, and conformational dynamics of the target proteins. Although structures and thermodynamics have been investigated extensively, very little experimental information has been reported about the conformational dynamics of de novo designed proteins.[24−26] A qualitative evaluation of dynamic properties, in some cases, can be obtained by superposing computed low-energy NMR structures. For example, Figure 1 compares the ensemble of structures of α-t-α,[21] which is stabilized only by hydrophobic interactions, with that of α_2D,[23] which is stabilized through the interaction of a diverse set of hydrophobic, aromatic, and polar side chains. Clearly, the structure of the α-t-α peptide is less well-defined than that of α_2D, suggesting that the α-t-α peptide samples a larger range of conformations in solution. However, apparent disorder of the ensemble can result from insufficient numbers of assigned NOEs or from the lack of stereospecific resonance assignments. Definitive determination of equilibrium conformational dynamic properties of a designed protein requires direct measurement, as illustrated in an elegant series of investigations of ubiquitin variants with repacked hydrophobic cores.[24−26]

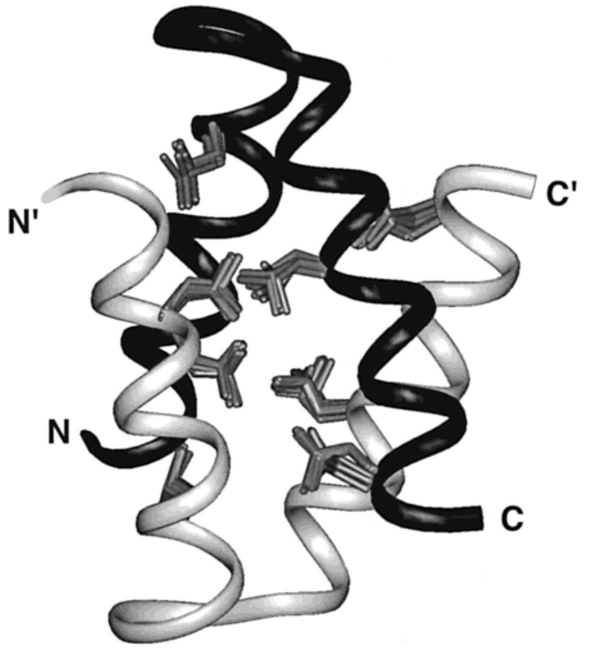

Figure 2. Structure of α_2D. The C^α backbone of α_2D is shown as a solid tube; the leucine side chains are shown as the superposition of the conformations observed in the 10 lowest energy NMR solution structures of α_2D.[23] α_2D was designed to be a dimeric four-helix bundle; it adopts the bisecting U motif. The figure was drawn from the coordinates of PDB file 1qp6 using InsightII (MSI Research).

The present investigation utilizes ^{13}C nuclear spin relaxation measurements to characterize the backbone conformational dynamics of the de novo designed protein α_2D on picosecond to nanosecond and microsecond to millisecond time scales. α_2D is a dimeric four-helix bundle whose structure, shown in Figure 2, is the most well-defined of the de novo designed proteins described to date.[23,27] This model protein has a structure typical of globular, native proteins; features important for its conformational specificity include a hydrophobically stabilized interface between helices 1 and 1′ and a hydrogen-bond-stabilized interface between helices 2 and 2′.[28]

Experimental and theoretical methods for characterizing protein dynamics from ^{13}C nuclear spin relaxation are not as widely applied as ^{15}N spectroscopic methods;[29,30] however, ^{13}C NMR spectroscopy is particularly well-suited to investigation of conformational dynamics of de novo designed proteins. First, small de novo designed proteins can be synthesized chemically. Thereby, selective enrichment with ^{13}C can be used to avoid complications from ^{13}C−^{13}C scalar and dipolar couplings encountered in proteins uniformly labeled with ^{13}C.[31−33] Second, ^{15}N NMR spectroscopy is rendered relatively more complicated by fast amide proton exchange with solvent for proteins with

---

(18) Ilyina, E.; Roongta, V.; Mayo, K. H. *Biochemistry* **1997**, *36*, 5245−5250.

(19) Skalicky, J.; Gibney, B.; Rabanal, F.; Urbauer, R.; Dutton, P.; Wand, A. *J. Am. Chem. Soc.* **1999**, *121*, 4941−4951.

(20) Schafmeister, C. E.; LaPorte, S. L.; Miercke, L. J.; Stroud, R. M. *Nat. Struct. Biol.* **1997**, *4*, 1039−1046.

(21) Fezoui, Y.; Connolly, P. J.; Osterhout, J. J. *Protein Sci.* **1997**, *6*, 1869−1877.

(22) Walsh, S. T. R.; Cheng, H.; Bryson, J. W.; Roder, H.; DeGrado, W. F. *Proc. Natl. Acad. Sci. U.S.A.* **1998**, *96*, 5486-5491.

(23) Hill, R. B.; DeGrado, W. F. *J. Am. Chem. Soc.* **1998**, *120*, 1138−1145.

(24) Lazar, G.; Johnson, E.; Desjarlais, J.; Handel, T. *Protein Sci.* **1999**, *8*, 2598−2610.

(25) Johnson, E.; Handel, T. *J. Biomol. NMR* **1999**, *15*, 135−143.

(26) Johnson, E.; Lazar, G.; Desjarlais, J.; Handel, T. *Struct. Folding Des.* **1999**, *7*, 967−976.

(27) Raleigh, D. P.; Betz, S. F.; DeGrado, W. F. *J. Am. Chem. Soc.* **1995**, *117*, 7558−7559.

(28) Hill, R. B.; Hong, J.-K.; DeGrado, W. F. *J. Am. Chem. Soc.* **2000**, *122*, 746−747.

(29) Kay, L. E. *Nat. Struct. Biol.* **1998**, *5*, 513−517.

(30) Palmer, A. G. *Curr. Opin. Struct. Biol.* **1997**, *7*, 732−737.

(31) Yamazaki, T.; Muhandiram, R.; Kay, L. E. *J. Am. Chem. Soc.* **1994**, *116*, 8266−8278.

(32) LeMaster, D. M.; Kushlan, D. *J. Am. Chem. Soc.* **1996**, *118*, 9255−9264.

(33) Wand, A. J.; Bieber, R. J.; Urbauer, J. L.; McEvoy, R. P.; Gan, Z. *J. Magn. Reson., Ser. B* **1995**, *108*, 173−175.

limited stabilities.[34] Third, ^{13}C chemical shifts, particularly for CO, C$^{\alpha}$, and C$^{\beta}$, are diagnostic of secondary structural preferences.[35,36] Fourth, dynamics of hydrophobic side chains can be investigated in order to assess hydrophobic core packing and stability.[24−26]

For the investigations reported herein, α_2D was enriched synthetically with ^{13}C at the C$^{\alpha}$ positions of the Leu residues 6, 13, 25, and 32. Each of these residues has a symmetry-related counterpart, 6′, 13′, 25′, and 32′, in the dimeric structure. These residues were selected specifically to evaluate whether α_2D displays conformational fluctuations typical of native biological globular proteins. The eight ^{13}C-labeled Leu residues are located in the hydrophobic core of the dimer and are spaced ideally along the backbone to serve as reporter groups for the motional properties of α_2D (Figure 2). Relaxation rate constants were recorded at static magnetic field strengths of 9.4, 11.7, 14.1, and 17.6 T. Picosecond to nanosecond time scale dynamics were characterized using reduced spectral density mapping and the model-free formalism. Microsecond to millisecond time scale dynamics were characterized using global analysis of rotating frame relaxation dispersion. The results indicate the success of the design strategy and illustrate how folding forces favor folded states over unfolded states of α_2D.

Methods

Sample Preparation. The free amine of L-leucine-*2*-^{13}*C* (Isotec) was protected with the 9-fluorenylmethyloxycarbonyl (Fmoc) group as follows: A 10-mL, pear-shaped flask was charged with L-leucine-*2*-^{13}*C* (131.2 mg, 1 mmol), diisopropylethylamine (DIEA) (174 μL, 1 mmol), and 4 mL of CH_3CN/H_2O (60%/40%). The mixture was stirred at room temperature, and *N*-(9-fluorenylmethyloxycarbonyl)oxysuccinimide (330.5 mg, 0.98 mmol) was added. The reaction was maintained at pH ~8 by the addition of 10% DIEA as necessary. The reaction was allowed to proceed for 4 h, and the product, Fmoc-L-leucine-*2*-^{13}*C*, was precipitated by addition to 1 N HCl at 0 °C and collected by filtration. The identity of the product was confirmed by NMR spectroscopy and mass spectrometry (yield = 94%). The polypeptide [6,13,25,32]L-leucine-*2*-^{13}*C*-α_2D (Ac-GEVEEL*EKKFKEL*WKGPRRG-EIEEL*HKKFHEL*IKG-NH_2) was synthesized using Fmoc-protected amino acids by standard solid-phase methods. The peptide was purified by high-performance liquid chromatography using a VYDAC C18 column. The level of incorporation of labeled leucine into α_2D was determined to be greater than 95% at each position by using electrospray mass spectrometry. All samples for NMR spectroscopy were prepared in 25 mM tris(hydroxymethyl)methylamine-d_{11} in 100% D_2O, pH 7.3 (uncorrected for deuterium isotope effects). Unless otherwise stated, sample concentrations were 2.0 mM.

NMR Spectroscopy. Relaxation experiments were performed at four magnetic field strengths on the following instruments: 9.4 T, a Bruker DRX400 equipped with a broad-band inverse probe (Swarthmore College); 11.7 T, a Bruker DRX500 equipped with a triple-resonance three-axis gradient probe (Columbia University); 14.1 T, a Bruker AMX600 equipped with a triple-resonance single-axis gradient probe (DuPont Pharmaceuticals) and a Bruker DRX600 equipped with a triple-resonance three-axis gradient probe (Columbia University); and 17.6 T, a Bruker DRX750 equipped with a triple-resonance three-axis gradient probe (NMRFAM, University of Wisconsin, Madison). All experiments were performed at 25 °C; temperatures were calibrated using a 100% methanol sample.[37] The HDO chemical shift relative to DSS was used to indirectly reference the ^{13}C dimension as described by Wishart and co-workers.[38] The proton carrier was set to the frequency of the water resonance, and the ^{13}C carrier frequency was set to 55 ppm. For typical two-dimensional spectra, spectral widths were 600 × 12 500 Hz in the $F1 \times F2$ dimensions, 128 × 1024 complex points were acquired in the $t_1 \times t_2$ dimensions, and 16−32 transients were accumulated per complex t_1 point. Coherence selection in the $F1$ indirect evolution periods used PEP echo/antiecho gradient or phase-cycled methods as appropriate.[39,40] NMR data were analyzed using in-house software and Felix 97 (MSI Research).

Laboratory Frame NMR Relaxation Measurements. The ^{13}C spin−lattice relaxation rate constant R_1, the spin−spin relaxation rate constant R_2, and the steady-state $\{^1H\}-^{13}C$ NOE were measured using inversion recovery, Carr−Purcell−Meiboom−Gill (CPMG), and steady-state NOE pulse sequences[41,42] with minor modifications for application to ^{13}C rather than ^{15}N. CPMG experiments used a spacing between 180° pulses of 0.5 ms. Steady-state NOE experiments used a 3.75-s train of 180° ^{1}H pulses with a spacing of 5 ms for saturation and a 4.85-s recycle delay for control experiments. Relaxation measurements at each field were performed in the order R_2−NOE−R_1−NOE. The R_1 and R_2 measurements were performed using 7−14 time points with delays chosen to fully define the exponential decay curve. For each R_1 or R_2 measurement, at least two time points were recorded in duplicate or triplicate for error analysis. NOE measurements were performed in duplicate for error analysis. All data were processed using the same protocol. Peak heights were extracted using FELIX 97 macros. Uncertainties in peak height measurements were estimated from pairwise analyses of duplicate or triplicate spectra as described previously.[42,43] The values of R_1 and R_2 and their associated uncertainties were determined by nonlinear least-squares optimization using the in-house program CurveFit. The time-series data were fit to a monoexponential decay function, $I(t) = I(0) \exp[-R_{1,2}t]$, in which $I(t)$ is the intensity of the resonance in the spectrum recorded with a relaxation time t. Uncertainties in the fitted rate constants were obtained from Monte Carlo simulations.[43,44] $\{^1H\}-^{13}C$ NOE values were determined as the ratios of peak intensities measured from spectra acquired with and without proton saturation. Uncertainties in the NOE values were determined by error propagation. The $^1H-^{13}C$ cross relaxation rate constant, σ_{CH}, was calculated as

$$\sigma_{CH} = R_1(\mathrm{NOE} - 1)\gamma_C/\gamma_H \tag{1}$$

NMR Relaxation Data Analysis. The relaxation of the carbon ^{13}C nucleus is dominated by the dipolar interaction with the attached proton and affected to lesser extent by the ^{13}C chemical shift anisotropy interaction.[45] Exact expressions for R_1, R_2, and σ_{CH} were approximated using reduced spectral density mapping according to the procedures of Farrow and co-workers,[46] with modifications for ^{13}C:[47,48]

$$R_1 = \frac{d^2}{4}[3J(\omega_C) + 7J(1.12\omega_H)] + c^2 J(\omega_C) \tag{2}$$

---

(34) Grzesiek, S.; Bax, A. *J. Am. Chem. Soc.* **1993**, *115*, 12593−12594.

(35) Wishart, D. S.; Bigam, C. G.; Holm, A.; Hodges, R. A.; Sykes, B. D. *J. Biomol. NMR* **1995**, *5*, 67−81.

(36) Spera, S.; Bax, A. *J. Am. Chem. Soc.* **1991**, *113*, 5490−5492.

(37) Cavanagh, J.; Fairbrother, W. J.; Palmer, A. G.; Skelton, N. J. *Protein NMR Spectroscopy: Principles and Practice*; Academic Press: San Diego, CA, 1996.

(38) Wishart, D. S.; Bigam, C. G.; Yao, J.; Abildgaard, F.; Dyson, H. J.; Oldfield, E.; Markley, J. L.; Sykes, B. D. *J. Biomol. NMR* **1995**, *6*, 135−140.

(39) Kay, L. E.; Keifer, P.; Saarinen, T. *J. Am. Chem. Soc.* **1992**, *114*, 10663−10665.

(40) Palmer, A. G.; Cavanagh, J.; Byrd, R. A.; Rance, M. *J. Magn. Reson.* **1992**, *96*, 416−424.

(41) Farrow, N. A.; Zhang, O.; Forman-Kay, J. D.; Kay, L. E. *Biochemistry* **1995**, *34*, 868−878.

(42) Skelton, N. J.; Palmer, A. G.; Akke, M.; Kördel, J.; Rance, M.; Chazin, W. J. *J. Magn. Reson., Ser. B* **1993**, *102*, 253−264.

(43) Palmer, A. G.; Rance, M.; Wright, P. E. *J. Am. Chem. Soc.* **1991**, *113*, 4371−4380.

(44) Press: W. H.; Flannery, B. P.; Teukolsky, S. A.; Vetterling, W. T. *Numerical Recipes. The Art of Scientific Computing*; Cambridge University Press: Cambridge, 1986.

(45) Abragam, A. *Principles of Nuclear Magnetism*; Clarendon Press: Oxford, 1961.

(46) Farrow, N. A.; Zhang, O.; Szabo, A.; Torchia, D. A.; Kay, L. E. *J. Biomol. NMR* **1995**, *6*, 153−162.

(47) Guenneugues, M.; Gilquin, B.; Wolff, N.; Menez, A.; Zinn-Justin, S. *J. Biomol. NMR* **1999**, *14*, 47−66.

(48) Atkinson, R. A.; Lefevre, J. F. *J. Biomol. NMR* **1999**, *13*, 83−88.

$$R_2 = \frac{d^2}{8}[4J(0) + 3J(\omega_C) + 13J(1.06\omega_H)] + \left(\frac{c^2}{6}\right)[4J(0) + 3J(\omega_C)] + \Delta R_2\left(\frac{1}{\tau_{cp}}\right) \quad (3)$$

$$\sigma_{CH} = \frac{5d^2}{4}J(1.56\omega_H) \quad (4)$$

in which $d = (\mu_0 h\gamma_H\gamma_C/8\pi^2)\langle r_{CH}^{-3}\rangle$, $c = \omega_C\Delta\sigma/3^{1/2}$, μ_0 is the permeability of free space, h is Planck's constant, γ_H and γ_C are the gyromagnetic ratios of ^{1}H and ^{13}C, respectively, $r_{CH} = 1.09$ Å is the average $C^\alpha-H^\alpha$ bond length, and $\Delta\sigma = 25$ ppm is the chemical shift anisotropy typical for $^{13}C^\alpha$ nuclei.[43] $\Delta R_2(1/\tau_{cp})$ is the residual chemical exchange term that takes into account kinetic processes that contribute to the observed R_2 rate constant under conditions of fast pulsing during the CPMG sequence. For $\tau_{cp} = 0.5$ ms and chemical shift differences between exchanging sites of less than 3 ppm, $\Delta R_2(1/\tau_{cp}) = \Theta_{ex}B_0^2$ for either fast or slow exchange, in which B_0 is the static magnetic field and Θ_{ex} is a constant of proportionality (vide infra). The power spectral density function, $J(\omega)$, defines the frequency spectrum of stochastic overall and intramolecular motions that reorient the $C^\alpha-H^\alpha$ bond. Reduced spectral density mapping assumes that $J(\omega)$ is a linear function of ω^{-2} between $J(\omega_H - \omega_C)$ and $J(\omega_H + \omega_C)$; consequently, linear combinations of the high-frequency spectral density terms, $J(\omega_H - \omega_C)$, $J(\omega_H)$, and $J(\omega_H + \omega_C)$ can be represented by a single term, $J(\beta\omega_H)$, with β chosen as in eqs 2−4. This assumption is valid if the time correlation function describing the dynamics of the C−H bond vector may be represented as a sum (or distribution) of exponential terms and if the exponential time constants, τ_i, satisfy either $(\omega_H + \omega_C)\tau_i \ll 1$ or $(\omega_H - \omega_C) \gg 1$. For static magnetic fields between 9.4 and 17.6 T, the constraints on the time constants are approximately satisfied if $\tau_i < 80$ ps or if $\tau_i < 1000$ ps, in which τ_i refers to either overall rotation or internal motions that reorient the C−H bond vector (vide infra).

Relaxation rate constants were measured at four static magnetic field strengths, $B_0 = 9.4$, 11.7, 14.1, and 17.6 T, corresponding to ^{1}H Larmor frequencies of $\omega_H = 2.51 \times 10^9$, 3.14×10^9, 3.77×10^9, and 4.71×10^9 s^{-1}. The measured σ_{CH} values were used to calculate $J(\omega)$ at the frequencies $\omega = 1.56\omega_H = 3.92 \times 10^9$, 4.90×10^9, 5.88×10^9, and 7.35×10^9 s^{-1} using eq 4. A linear least-squares fit of $J(\omega)$ versus ω^{-2} was used to predict $J(\omega)$ at other frequencies near ω_H, as needed for determining $J(0)$ and $J(\omega_C)$. Values of $J(\omega_C)$ were obtained directly from R_1 by using eq 2. To avoid extrapolations beyond the measured range of frequencies when estimating $J(1.12\omega_H)$, only the R_1 values recorded at $B_0 = 14.1$ and 17.6 T were utilized. Direct inversion of eq 3 to determine $J(0)$ is not possible because of possible contributions from $\Delta R_2(1/\tau_{cp})$; instead, $J(0)$ was obtained by defining[49]

$$\Gamma = R_2 - \frac{1}{2}R_1 - \frac{3d^2}{4}J(\omega_H) = \frac{d^2}{2}J(0) + \left(\frac{2}{9}\gamma_C^{\,2}\Delta\sigma^2 J(0) + \Theta_{ex}\right)B_0^{\,2} \quad (5)$$

Data from all four fields were used to determine values of $J(\omega_H)$ needed in eq 5, even though extrapolation was required for $B_0 = 9.4$ and 11.7 T, because contributions to Γ from $J(\omega_H)$ are very small (<1%).The value of $J(0)$ is obtained from the intercept of a linear least-squares fit of Γ versus B_0^2.

The model-free spectral density function derived by Lipari and Szabo[50] and extended by Clore and co-workers,[51]

$$J(\omega) = \frac{2}{5}\left[\frac{S^2\tau_m}{1 + (\omega\tau_m)^2} + \frac{(1 - S_f^{\,2})\tau_f'}{1 + (\omega\tau_f')^2} + \frac{(S_f^{\,2} - S^2)\tau_s'}{1 + (\omega\tau_s')^2}\right] \quad (6)$$

was used in all data analyses. In eq 6, $\tau_f' = \tau_f\tau_m/(\tau_f + \tau_m)$, $\tau_s' = \tau_s\tau_m/(\tau_s + \tau_m)$, τ_m is the local overall rotational correlation time of the molecule (vide infra), τ_f is the effective correlation time for internal motions on a fast time scale defined by $\tau_f < 100-200$ ps, τ_s is the effective correlation time for internal motions on a slow time scale of ∼1 ns defined by $\tau_f < \tau_s < \tau_m$, $S^2 = S_f^2S_s^2$ is the square of the generalized order parameter characterizing the amplitude of the internal motions, and S_f^2 and S_s^2 are the squares of the order parameters for the internal motions on the fast and slow time scales, respectively. Generalized order parameters quantify the amplitudes of motions of the $H^\alpha-C^\alpha$ bond vector on the picosecond to nanosecond time scale, with values ranging from zero for isotropic internal motions to unity for completely restricted motion in a molecular reference frame.

Numerical simulations were used to evaluate the accuracy of the reduced spectral density mapping protocol. Five hundred simulated relaxation data sets were generated by randomly selecting S_f^2 and S_s^2 from a uniform distribution between 0 and 1. Simulated values of $J(\omega)$ were calculated from S_f^2 and S_s^2 using eq 6 with $\tau_m = 4.7$ ns, $\tau_s = 1$ ns, and $\tau_f = 80$ ps. Relaxation rate constants R_1, R_2, and σ_{CH} values at static field strengths of 9.4, 11.7, 14.1, and 17.6 T were calculated from the simulated $J(\omega)$. Reduced spectral density values were determined from the simulated relaxation data sets using eqs 2, 4, and 5.

Local overall rotational correlation times and the amplitudes and time scales of intramolecular motions for the Leu ^{13}C spins in α_2D were obtained by fitting eq 6 to the experimental values of $J(\omega)$, determined by reduced spectral density mapping. Nonlinear least-squares optimization was performed by using the program CurveFit as follows: first, the data were fit with τ_m and S_f^2 only by assuming that $S_s^2 = 1$ and $\tau_f = 0$ (model 1); second, the data were fit with τ_m, S_f^2, and τ_f assuming $S_s^2 = 1$ (model 2); and third, the data were fit with τ_m, S_f^2, S_s^2, and τ_s by assuming $\tau_f = 0$. Discrimination between models was performed using an F-test.[52,53]

For comparison, eq 6 also was fit directly to the relaxation rate constants, without the intervening determination of reduced spectral density values, using the in-house program ModelFree (version 4.10).[53] The same spectral density models were used for this analysis as above, except that a contribution $\Delta R_2(1/\tau_{cp}) = \Theta_{ex}B_0^2$ was included in all models and Θ_{ex} was optimized along with the model-free parameters. A single global overall value of τ_m was optimized along with the internal motional parameters. To allow a direct comparison with the model-free parameters obtained from fitting the reduced spectral density values, R_1 data acquired at $B_0 = 9.4$ and 11.7 T were not included in the analysis.

Relaxation-Compensated CPMG Experiments. As discussed below, the B_0 dependence of Γ (eq 5) suggested that all Leu residues were subject to chemical exchange broadening. To confirm this result, chemical exchange contributions to R_2 were characterized using relaxation-compensated CPMG experiments[54] at $B_0 = 11.7$ T. $R_2(1/\tau_{cp})$ relaxation rate constants were measured using τ_{cp} delays of 0.50, 0.68, 1.00, 1.25, 2.00, 3.36, 5.00, and 6.70 ms, using the same 2.0 mM sample used for laboratory frame relaxation experiments. This sample was diluted and $R_2(1/\tau_{cp})$ was measured for $\tau_{cp} = 0.5$ and 10.0 ms at α_2D monomer concentrations of 1.0 and 0.5 mM. Subsequently, chemical exchange contributions to R_2 were characterized more completely using relaxation-compensated CPMG pulse experiments recorded at $B_0 = 11.7$ and 14.1 T with a new 1.7 mM sample. $R_2(1/\tau_{cp})$ relaxation rate constants were measured using τ_{cp} delays of 0.50, 0.67, 1.00, 2.00, 4.00, 7.14, 14.28, and 42.84 ms; the $\tau_{cp} = 0.67$ ms data set was recorded at 14.1 T only. Experiments for $\tau_{cp} \leq 4.00$ ms used the original relaxation-compensated pulse sequence.[54] At each value of τ_{cp}, 8−10 spectra were recorded, including two duplicate measurements in order to define the relaxation decay curve. Experiments for $\tau_{cp} = 7.14$ and 14.28 ms used the self-compensated pulse sequence recently described.[55] For $\tau_{cp} = 7.14$ ms, six spectra were recorded, including two duplicate measurements in order to define the relaxation

---

[49] Phan, I. Q. H.; Boyd, J.; Campbell, I. D. *J. Biomol. NMR* **1996**, *8*, 369−378.

[50] Lipari, G.; Szabo, A. *J. Am. Chem. Soc.* **1982**, *104*, 4546−4559.

[51] Clore, G. M.; Szabo, A.; Bax, A.; Kay, L. E.; Driscoll, P. C.; Gronenborn, A. M. *J. Am. Chem. Soc.* **1990**, *112*, 4989−4991.

[52] Devore, J. *Probability and Statistics for Engineering and the Sciences*; Brooks/Cole Publishing Co.: Monterey, CA, 1982.

[53] Mandel, A. M.; Akke, M.; Palmer, A. G. *J. Mol. Biol.* **1995**, *246*, 144−163.

[54] Loria, J.; Rance, M.; Palmer, A. *J. Am. Chem. Soc.* **1999**, *121*, 2331−2332.

[55] Millet, O.; Loria, J. P.; Kroenke, C. D.; Pons, M.; Palmer, A. G. *J. Am. Chem. Soc.* **2000**, *122*, 2867−2877.

decay curve. For $\tau_{cp} = 14.28$ ms, two spectra were recorded with a relaxation period of 0 ms, and 10 spectra were recorded with a relaxation period of 28.56 (14.1 T) or 57.12 ms (11.7 T). Experiments for 42.84 ms used the Hahn echo pulse sequence recently described.[55] Two spectra were recorded with a relaxation period of 0 ms, and 10 spectra were recorded with a relaxation period of 42.84 ms. Spectra were processed in a similar fashion as the R_1 and R_2 experiments. Time series data obtained for τ_{cp} values from 0.50 to 7.14 ms were fit using the in-house program CurveFit to a monoexponential decay function, $I(t) = I(0)\exp[-R_2(1/\tau_{cp})t]$, in which $I(t)$ is the intensity of the resonance in the spectrum recorded with a relaxation time t. Experimental uncertainties in the peak intensities were estimated from duplicate spectra.[42,43] Uncertainties in the fitted rate constants were obtained from Monte Carlo simulations.[44] For τ_{cp} values of 14.28 and 42.84 ms, rate constants were obtained from $R_2(1/\tau_{cp}) = \ln[\langle I(0)\rangle/\langle I(t)\rangle]/t$, in which t is the nonzero relaxation delay, $\langle I(0)\rangle$ is the mean intensity in the spectrum recorded with a relaxation delay of zero, and $\langle I(t)\rangle$ is the mean intensity for the duplicate spectra recorded at the nonzero relaxation delay. Uncertainties in $\langle I(t)\rangle$ were taken to be the standard error in the mean. $I(0)$ was assumed to have the same relative uncertainty as the set of $I(t)$ values.

Chemical Exchange Data Analysis. A two-site chemical exchange reaction between dimeric and monomeric forms of α_2D is considered (vide infra),

$$\mathrm{D} \underset{k_{-1}}{\overset{k_1}{\rightleftharpoons}} 2\mathrm{M} \tag{7}$$

in which $d[D]/dt = -(1/2)d[M]/dt = k_{-1}[M]^2 - k_1[D]$, k_1 is the forward first-order kinetic rate constant (unfolding off-rate), and k_{-1} is the reverse second-order kinetic rate constant (folding on-rate). The equilibrium disassociation constant $K_d = k_1/k_{-1}$, the equilibrium fraction of monomeric α_2D molecules is $p_M = [M]/([M] + 2[D])$, and the equilibrium fraction of α_2D molecules in dimers is $p_D = 1 - p_M$. In the present case, $p_D \gg p_M$. A general expression for the phenomenological transverse relaxation rate constant for the dimeric species, $R_2(1/\tau_{cp})$, is given by[56,57]

$$R_2\left(\frac{1}{\tau_{cp}}\right) = R_2^{\,0} + \frac{1}{2}\left(k_{ex} - \frac{1}{\tau_{cp}}\cosh^{-1}[D_+\cosh(\eta_+) - D_-\cos(\eta_-)]\right) \tag{8}$$

in which $k_{ex} = 2[M]k_{-1} + k_1 = k_1/p_M = 2[M]k_{-1}/p_D$, $D_\pm = \pm(1/2) + (k_{ex}^2 + \Delta\omega^2)/2\zeta$, $\eta_\pm = 2^{-1/2}\tau_{cp}[\pm(k_{ex}^2 - \Delta\omega^2) + \zeta]^{1/2}$, $\zeta^2 = (k_{ex}^2 + \Delta\omega^2)^2 - 16p_Mp_Dk_{ex}^2\Delta\omega^2$, and τ_{cp} is the delay between 180° pulses in the CPMG pulse train. The two sites (unfolded monomer and folded dimer) are assumed to have distinct chemical shifts ω_M and ω_D, respectively, and $\Delta\omega = |\omega_M - \omega_D|$. The average transverse relaxation rate constant due to dipolar and CSA interactions is denoted $R_2^\circ = R_2(1/\tau_{cp} \to \infty)$. Equation 8 assumes $|R_M - R_D| \ll \Delta\omega$, in which R_M is the relaxation rate constant for the monomer and R_D is the relaxation rate constant for the dimer. The amplitude of the relaxation dispersion is defined as $R_{ex} = R_2(1/\tau_{cp} \to 0) - R_2^0$.

The $R_2(1/\tau_{cp})$ data acquired at static magnetic fields of 11.7 and 14.1 T were fit simultaneously to eq 8, assuming that $\Delta\omega$ scales linearly with the static magnetic field strength. The independent fitting parameters were R_2^0, p_Mp_D, k_{ex}, and the value of $\Delta\omega$ at 11.7 T. For simplicity, the very small field-dependent contribution to R_2^0 from CSA relaxation was ignored. Fitting was performed with the in-house program CPMGfit assuming equal weights for all $R_2(1/\tau_{cp})$ values; uncertainties in fitted parameters were obtained by jackknife simulations.[58]

The value of $\Delta R_2(1/\tau_{cp})$ used in eqs 3 and 5 is given by eq 8 as $\Delta R_2(1/\tau_{cp}) = R_2(1/\tau_{cp}) - R_2^0$, in which $\tau_{cp} = 0.5$ ms. For skewed populations of the exchanging species ($p_D \gg p_M$) and fast pulsing in the CPMG experiment ($1.5/\tau_{cp} = 3000$ s$^{-1} > \Delta\omega$), both of which are conditions satisfied for the present investigations of α_2D (vide infra), $\Delta R_2(1/\tau_{cp}) \approx p_Mp_D\Delta\omega^2k_{ex}/(k_{ex}^2 + 12/\tau_{cp}^2)$.[59] Because $\Delta\omega \propto B_0$, $\Delta R_2(1/\tau_{cp}) \propto B_0^2$ for all values of k_{ex}. Therefore, the quadratic field dependence of $\Delta R_2(1/\tau_{cp})$ acquired with a single value of $\tau_{cp} = 0.5$ ms can be used to identify an exchange process but does not provide information on the time scale of exchange.[55]

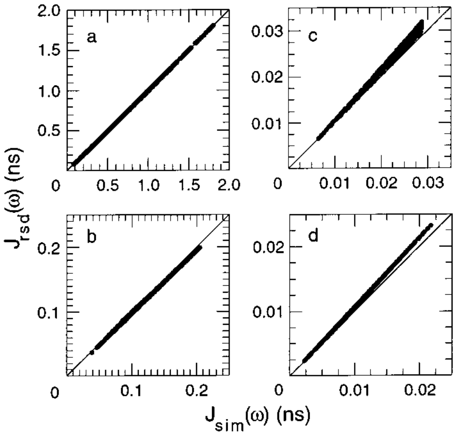

Figure 3. Numerical simulations of reduced spectral density mapping. Reduced spectral density values, $J_{rsd}(\omega)$, calculated from simulated relaxation data are compared to the actual simulated values of the spectral density function, $J_{sim}(\omega)$, for values of ω equal to (a) 0, (b) 0.95×10^9, (c) 3.92×10^9, and (d) 7.35×10^9 s^{-1}. The frequencies shown correspond to (b) ω_C at $B_0 = 14.1$ T, (c) $1.56\omega_H$ at $B_0 = 9.4$ T, and (d) $1.56\omega_H$ at $B_0 = 17.6$ T.

Results

NMR Spectroscopy and ^{13}C Chemical Shifts. All experiments were performed on samples specifically ^{13}C$^\alpha$-labeled at Leu 6, Leu 13, Leu 25, and Leu 32 (and the symmetry-related positions Leu 6′, Leu 13′, Leu 25′, and Leu 32′). The ^{13}C$^\alpha$ chemical shift assignments for α_2D were obtained from heteronuclear ^{1}H$-$^{13}C correlation spectroscopy using the ^{1}H$^\alpha$ chemical shift assignments previously determined.[23] The ^{13}C resonance assignments for the folded dimeric α_2D molecule are as follow: Leu 6, 58.1 ppm; Leu 13, 57.6 ppm; Leu 25, 58.1 ppm; Leu 32, 57.7 ppm. The ^{13}C$^\alpha$ chemical shift for amino acid residues in helical conformations is downfield of the random coil ^{13}C$^\alpha$ chemical shift and is diagnostic for secondary structure elements in proteins.[35,36] The canonical random coil chemical shift of a Leu ^{13}C$^\alpha$ is reported to be 55.7 ppm.[35,36] Therefore, the observed Leu ^{13}C$^\alpha$ chemical shifts for α_2D resonate downfield 1.9−2.4 ppm from the random coil value and are consistent with the highly helical structure of α_2D.

Molecular motions of the backbone of α_2D on picosecond to nanosecond time scales were characterized using the ^{13}C spin−lattice relaxation rate constant R_1, the ^{13}C spin−spin relaxation constant R_2, and the heteronuclear cross relaxation rate constant σ_{CH}, measured at four static magnetic field strengths, $B_0 = 9.4$, 11.7, 14.1, and 17.6 T, for a 2.0 mM monomer (1.0 mM dimer) α_2D sample. The relaxation rate constants are given in the Supporting Information.

Spectral Density Mapping. Numerical simulations were used to evaluate the accuracy and range of applicability of reduced spectral density mapping. The reduced spectral density values determined from simulated relaxation data are compared to the simulated values of $J(\omega)$ in Figure 3. The results are illustrated for $\tau_m = 4.7$ ns, $\tau_s = 1$ ns, and $\tau_f = 80$ ps. The errors in $J(0)$ are negligible for all combinations of S_f^2 and S_s^2. At ^{13}C and ^{1}H Larmor frequencies, the maximum deviations between the

---

(56) Davis, D. G.; Perlman, M. E.; London, R. E. *J. Magn. Reson., Ser. B* **1994**, *104*, 266−275.

(57) Jen, J. *J. Magn. Reson.* **1978**, *30*, 111−128.

(58) Mosteller, F.; Tukey, J. W. *Data Analysis and Regression. A Second Course in Statistics*; Addison-Wesley: Reading, MA, 1977.

(59) Ishima, R.; Torchia, D. A. *J. Biomol. NMR* **1999**, *15*, 369−372.

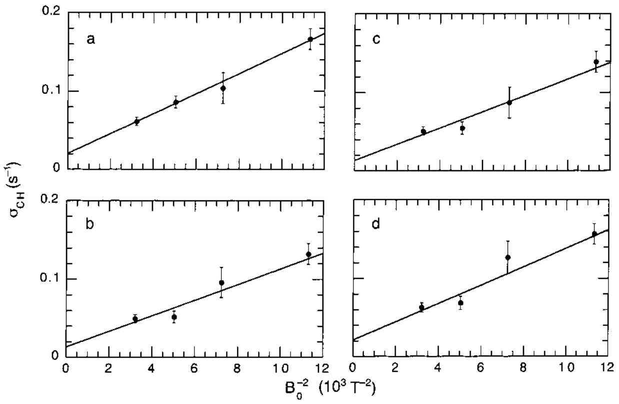

Figure 4. Reduced spectral density mapping characterizes the backbone motions of α_2D. Experimental values of cross-relaxation rates, σ_{CH}, versus the magnetic field strength, B_0^{-2}, for (a) Leu 6, (b) Leu 13, (c) Leu 25, and (d) Leu 32. The solid lines are linear least-squares fits to the experimental data. Fitted parameters are (a) slope = 0.0127 ± 0.0017 s^{-1} T^2, intercept = 0.020 ± 0.009 s^{-1}, $\chi^2 = 0.26$; (b) slope = 0.0099 ± 0.0015 s^{-1} T^2, intercept = 0.013 ± 0.008 s^{-1}, $\chi^2 = 3.42$; (c) slope = 0.0104 ± 0.0017 s^{-1} T^2, intercept = 0.013 ± 0.009 s^{-1}, $\chi^2 = 2.89$; and (d) slope = 0.0117 ± 0.0017 s^{-1} T^2, intercept = 0.021 ± 0.009 s^{-1}, $\chi^2 = 3.37$. Linearity of the plot is necessary for using reduced spectral density mapping to analyze $^{13}C^{\alpha}$ relaxation data for α_2D.

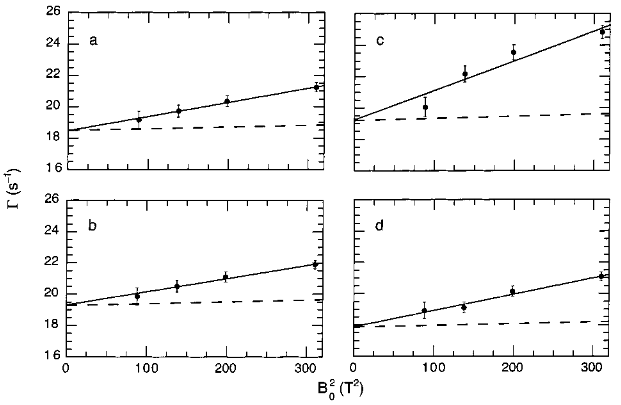

Figure 5. Chemical exchange contributions to spin relaxation in α_2D. Experimental values of Γ calculated using eq 5 are plotted versus B_0^2 for (a) Leu 6, (b) Leu 13, (c) Leu 25, and (d) Leu 32. The solid lines are linear least-squares fits to the experimental data. Fitted parameters are (a) slope = 0.0090 ± 0.0023 s^{-1} T^{-2}, intercept = 18.5 ± 0.5 s^{-1}, $\chi^2 = 0.12$; (b) slope = 0.0084 ± 0.0021 s^{-1} T^{-2}, intercept = 19.3 ± 0.5 s^{-1}, $\chi^2 = 0.31$; (c) slope = 0.0189 ± 0.0029 s^{-1} T^{-2}, intercept = 19.2 ± 0.6 s^{-1}, $\chi^2 = 4.02$; and (d) slope = 0.0104 ± 0.0021 s^{-1} T^{-2}, intercept = 17.9 ± 0.5 s^{-1}, $\chi^2 = 0.80$. The *y*-intercepts are proportional to $J(0)$, and the slopes depend on both the magnitude of the $^{13}C^{\alpha}$ CSA and chemical exchange contributions to R_2. The dashed lines show the field dependence of Γ predicted from eq 5 in the absence of chemical exchange linebroadening.

Table 1. Reduced Spectral Densities $J(\omega)$ for α_2D[a]

	ω (10^9 s^{-1})						
residue	0	0.95	1.18	3.92	4.90	5.88	7.35
Leu 6	1720 ± 50	82.5 ± 1.3	55.9 ± 1.2	6.2 ± 0.5	3.9 ± 0.7	3.2 ± 0.3	2.3 ± 0.2
Leu 13	1800 ± 50	83.3 ± 1.3	56.7 ± 1.0	4.9 ± 0.5	3.6 ± 0.7	1.9 ± 0.3	1.8 ± 0.2
Leu 25	1790 ± 60	85.6 ± 1.6	57.0 ± 1.4	5.2 ± 0.5	3.2 ± 0.7	2.0 ± 0.3	1.9 ± 0.2
Leu 32	1660 ± 40	90.6 ± 1.5	62.9 ± 1.1	5.8 ± 0.5	4.7 ± 0.8	2.6 ± 0.3	2.3 ± 0.2

[a] Table entries are $J(\omega)$ in units of picoseconds at the indicated frequencies ω.

actual and calculated $J(\omega)$ occur for the largest values of $J(\omega)$, when $S_f^2 \rightarrow 1$ and $S_s^2 \rightarrow 0$; under these conditions, the relaxation is dominated by the intermediate time scale process with τ_s = 1 ns. Errors in $J(\omega_C)$ are less than 5% at B_0 = 14.1 and 17.6 T, and errors in $J(1.56\omega_H)$ are less than 10% at B_0 = 9.4 T and less than 5% at the other three static fields. The reduced spectral density mapping approach becomes less accurate as τ_f is increased or τ_s is decreased. The value of $J(1.56\omega_H)$ obtained for B_0 = 9.4 T is most severely affected and generally should not be included in subsequent analyses of the reduced spectral density values. Simulated reduced spectral density mapping results for $J(\omega_C)$ at B_0 = 14.1 and 17.6 T and $J(1.56\omega_H)$ at B_0 = 11.7, 14.1, and 17.6 T still have maximum errors of <5% for τ_m = 4.7 ns, τ_s = 0.8 ns, and τ_f = 100 ps (not shown).

Reduced spectral densities, $J(\omega)$, were calculated from the relaxation rate constants using the reduced spectral density mapping approach embodied by eqs 2, 4, and 5. As shown by Figure 4, σ_{CH} were linear functions of B_0^{-2} for all residues over the range of B_0 = 9.4−17.6 T; consequently, the major assumption necessary for utilizing the reduced spectral density mapping approach of eqs 2−5 is satisfied. The σ_{CH} data for B_0 = 17.6 T are the most critical for determining the value of the *y*-intercept because B_0^{-2} is at its minimum value. Indeed, if the data for B_0 = 17.6 T are excluded, then the *y*-intercepts for residues Leu 13, Leu 25, and Leu 32 cannot be statistically distinguished from zero. All *y*-intercepts are positive, which is consistent with the theoretical expectation that the intercept is $0.4(1 - S^2)\tau_f$ in the limit that all intramolecular motions are very fast ($S_s^2 = 1$). These results emphasize the importance of data acquired at ultrahigh static magnetic fields for accurate analysis. The large slopes and nonzero intercepts observed in Figure 4 mean that the $J(\beta\omega_H)$ for different values of β in eqs 2−5 cannot be approximated by a single frequency-independent value $J(1.56\omega_H)$ derived from σ_{CH} (eq 4) or by $J(\beta\omega_H) = (1.56/\beta)^2 J(1.56\omega_H)$; rather, $J(\beta\omega_H)$ was obtained empirically from a linear least-squares fit to the observed frequency dependence.

Plots of Γ versus B_0^2, shown in Figure 5, were linear; however, the slopes of the graphs are too large to be attributed to the field dependence of CSA relaxation for $\Delta\sigma$ = 25 ppm. These results suggest that the measured values of R_2 contain a contribution from $\Delta R_2(1/\tau_{cp})$ (eq 3) for all Leu residues. The importance of eq 5 for determining $J(0)$ accurately is illustrated by the results for Leu 13 and 25. These residues have indistinguishable values of $J(0)$, even though R_2 for Leu 25 is significantly greater at all B_0 fields due to the larger exchange contributions to Leu 25.

The final values of the reduced spectral density values are given in Table 1. The $J(\omega)$ values for the two interior residues, Leu13, and 25, are very similar to one another, while the terminal residues, Leu 6 and 32, have smaller values of $J(0)$ and larger values of $J(\omega)$ at the highest frequencies.

Model-Free Formalism. The spectral density data for each Leu residue were interpreted using the Lipari−Szabo model-free formalism (eq 6) to obtain the rotational correlation time τ_m, order parameters S^2, and effective correlation times τ_f or τ_s for α_2D. As discussed above, $J(1.56\omega_H)$ for B_0 = 9.4 T is expected to be the least accurate value obtained from the reduced spectral density mapping procedure. Nonetheless, this value was included in the model-free analysis for α_2D, because statistically indistinguishable results were obtained when it was omitted (not shown). Data for Leu 13 and Leu 25 were adequately fit by the simplest spectral density function, model 1 (S_f^2, τ_m). Data for Leu 6 were not well-fit by model 1, and a significant improvement ($F = 64.6$, $p = 4.8 \times 10^{-4}$) was obtained using model 2 (S_f^2, τ_f, τ_m). Data for Leu 32 could not be fit with simple models

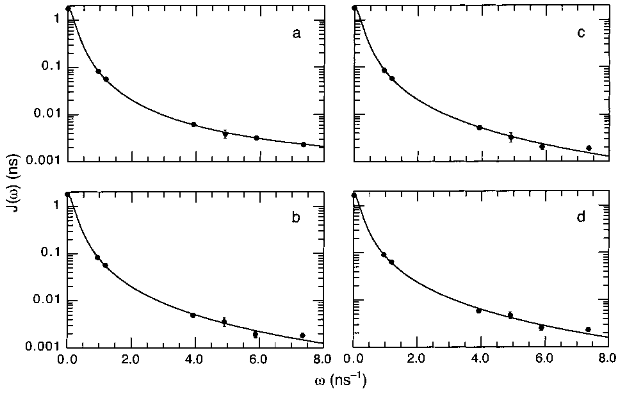

Figure 6. Amplitudes and time scales of the backbone motions of α_2D. Values of $J(\omega)$ derived from reduced spectral density mapping of $^{13}C^{\alpha}$ relaxation measurements at four magnetic field strengths are plotted versus frequency ω for (a) Leu 6, (b) Leu 13, (c) Leu 25, and (d) Leu 32. Solid lines are best fits to model spectral density functions derived from the Lipari–Szabo model-free formalism, eq 6, using a rotational correlation time $\tau_m = 4.71 \pm 0.05$ ns. Values of χ^2 are (a) 1.98, (b) 9.38, (c) 5.70, and (d) 9.86. Fitted order parameters and effective internal correlation times are given in Table 2.

Table 2. Model-Free Parameters for α_2D

residue	model	S^2	S_f^2	S_s^2	τ_f (ps)	τ_s (ns)
Leu 6	RSD-2[a]	0.918 ± 0.012	0.918 ± 0.012		28 ± 7	
	MF-2[b]	0.909 ± 0.011	0.909 ± 0.011		29 ± 3	
Leu 13	RSD-1	0.946 ± 0.011	0.946 ± 0.011			
	MF-1	0.932 ± 0.010	0.932 ± 0.010			
Leu 25	RSD-1	0.959 ± 0.014	0.959 ± 0.014			
	MF-1	0.948 ± 0.012	0.948 ± 0.012			
Leu 32	RSD-3	0.868 ± 0.038	0.933 ± 0.017	0.930 ± 0.023		1.12 ± 0.53
	MF-3	0.855 ± 0.026	0.919 ± 0.016	0.930 ± 0.014		0.82 ± 0.25

[a] RSD-N indicates that internal motional parameters were obtained by fitting reduced spectral densities with model N derived from eq 6. Analysis was performed using a fixed value of $\tau_m = 4.71 \pm 0.05$ ns. [b] MF-N indicates that internal motional parameters were obtained by fitting relaxation rate constants with model N derived from eq 6. The analysis was performed using the program ModelFree (version 4.10) and yielded an optimized value of $\tau_m = 4.72 \pm 0.04$ ns.

and gave very large uncertainties for more complex models. The values of $\tau_m = 4.69 \pm 0.08$, 4.74 ± 0.07, and 4.68 ± 0.09 ns obtained for Leu 6, Leu 13, and Leu 25, respectively, were very similar.

The structure of α_2D has relative moments of inertia (in the absence of hydration) of 1.00:0.89:0.69 and is expected to diffuse approximately as a prolate ellipsoid with $D_{\parallel}/D_{\perp} < 1.25$, in which $D_{\parallel}$ and $D_{\perp}$ are the principal values of the diffusion tensor.[60] The local overall correlation times experienced by ^{13}C spins in a moderately anisotropic molecule ($D_{\parallel}/D_{\perp} < 2$) are given by $\tau_m = \tau_{iso}/[1 - rY_{20}(\theta)]$, in which $\tau_{iso} = 1/(2D_{\parallel} + 4D_{\perp})$, $r = (D_{\parallel} - D_{\perp})/(D_{\parallel} + 2D_{\perp})$, $Y_{20}(\theta) = (3\cos^2\theta - 1)/2$, and θ is the angle between the symmetry axis of the diffusion tensor and the C–H bond vector.[61] The symmetry axis of the diffusion tensor is coincident with the dimer symmetry axis of α_2D. The angles θ are 50°, 64°, 66°, and 66°, and the expected values of τ_m are $1.01\tau_{iso}$, $0.98\tau_{iso}$, $0.98\tau_{iso}$, and $0.98\tau_{iso}$ for Leu 6, Leu 13, Leu 25, and Leu 32, respectively. All values of τ_m are close to τ_{iso} because all values of θ are close to the magic angle 54.7°; as a result, the Leu C–H vectors are insensitive to the anisotropy of rotational diffusion in α_2D.

The spectral density data were analyzed a second time using a fixed value of $\tau_m = 4.71 \pm 0.05$ ns for all Leu residues, because the range of τ_m values estimated from the orientations of the C–H vectors is less than the experimental uncertainties in the measured values. Essentially identical results were obtained for Leu 6, Leu 13, and Leu 25 by either optimizing or fixing τ_m. With τ_m fixed, data for Leu 32 were not well-fit by model 1 (S_f^2) or model 2 (S_f^2, τ_f), and a significant improvement ($F = 17.6$, $p = 0.010$) was obtained using model 3 (S_f^2, S_f^2, τ_s) compared to model 1. The final fits of the model spectral density functions are shown in Figure 6, and the fitted parameters are given in Table 2. Results from the direct analysis of the relaxation rate constants using the ModelFree program also are given in Table 2. The order parameters for the two interior residues, Leu 13 and 25, are large and very similar to one another. The terminal residues, Leu 6 and 32, have smaller order parameters, and, in addition, the internal correlation times are sufficiently large to contribute significantly to the spectral density function.

Direct Measurement of Chemical Exchange. As shown in Figure 5, the dependence of Γ on B_0^2 leads to the conclusion that all Leu residues in α_2D are subject to chemical exchange processes on the microsecond to millisecond time scale. The slope of the graph of Γ versus B_0^2 is greatest for Leu 25, which implies a larger degree of exchange linebroadening for this residue. To characterize fully the chemical exchange contributions to transverse relaxation, ^{13}C $R_2(1/\tau_{cp})$ relaxation rate constants were measured using relaxation-compensated CPMG pulse sequences. Values of $R_2(1/\tau_{cp})$ measured at 11.7 T using a 2.0 mM sample showed a strong dependence on τ_{cp} between 0.5 and 6.7 ms for all residues (data not shown). The relaxation dispersion provides definitive evidence that each of the Leu residues in α_2D participates in a chemical exchange process.

The physical basis for the exchange phenomenon was determined from the concentration dependence of the linebroadening. If exchange results from intramolecular conformational dynamics, then R_{ex} should be independent of concentration. If exchange arises from the folding equilibrium between the (unfolded) monomeric and (folded) dimeric forms of α_2D, then R_{ex} should decrease with an increase in sample concentration, because the relative population of the monomer decreases. If exchange results from aggregation to form higher order oligomers, then R_{ex} should increase with an increase in sample concentration, because the relative population of the oligomers increases.[62] The values of $R_2(1/\tau_{cp} = 0.1\ \text{ms}^{-1})$ and $R_2(1/\tau_{cp} = 1\ \text{ms}^{-1})$ measured for 0.5, 1.0, and 2.0 mM α_2D samples (monomer concentration) are shown in Figure 7. The difference $R_2(1/\tau_{cp} = 0.1\ \text{ms}^{-1}) - R_2(1/\tau_{cp} = 1\ \text{ms}^{-1})$, which was used to approximate the degree of exchange linebroadening, decreases with increasing sample concentration. These results indicate that a significant component of the exchange linebroadening results from the folding equilibrium for α_2D.

The kinetics of the chemical exchange process were characterized by measuring ^{13}C $R_2(1/\tau_{cp})$ relaxation dispersion curves as a function of τ_{cp} at $B_0 = 11.7$ and 14.1 T for a 1.7 mM

---

(60) Copié, V.; Tomita, Y.; Akiyama, S. K.; Aota, S.; Yamada, K. M.; Venable, R. M.; Pastor, R. W.; Krueger, S.; Torchia, D. A. *J. Mol. Biol.* **1998**, *277*, 663–682.

(61) Lee, L. K.; Rance, M.; Chazin, W. J.; Palmer, A. G. *J. Biomol. NMR* **1997**, *9*, 287–298.

(62) Pfuhl, M.; Chen, H. A.; Kristensen, S. M.; Driscoll, P. C. *J. Biomol. NMR* **1999**, *14*, 307–320.

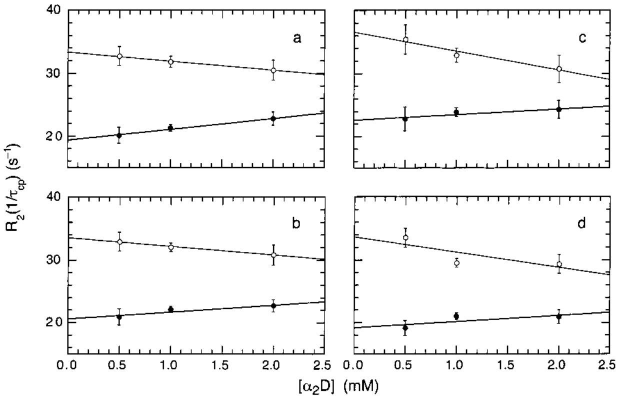

Figure 7. Folding equilibrium causes chemical exchange in α_2D. Values of $R_2(1/\tau_{cp})$ for (●) $\tau_{cp} = 0.5$ ms and (○) $\tau_{cp} = 10.0$ ms are plotted versus the total monomer concentration of α_2D for (a) Leu 6, (b) Leu 13, (c) Leu 25, and (d) Leu 32. Values of $R_2(1/\tau_{cp})$ at $\tau_{cp} = 10.0$ ms for 2.0 mM α_2D were obtained by extrapolating the relaxation dispersion curves measured for τ_{cp} values ranging from 6.7 to 0.5 ms (data not shown). The solid lines are drawn to guide the eye. The difference between the two values of $R_2(1/\tau_{cp})$ at a given τ_{cp} is an approximate indication of the chemical exchange contribution to transverse relaxation. The decreased chemical exchange linebroadening at higher protein concentrations identifies the folding equilibrium for α_2D to be the mechanism for exchange linebroadening.

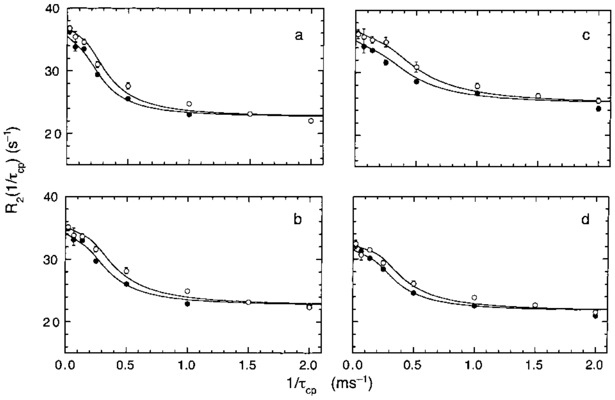

Figure 8. Determination of protein folding parameters for α_2D from the field dependence of CPMG relaxation dispersion. Values of $R_2(1/\tau_{cp})$ measured at (●) $B_0 = 11.7$ T and (○) $B_0 = 14.1$ T are plotted versus $1/\tau_{cp}$ for (a) Leu 6, (b) Leu 13, (c) Leu 25, and (d) Leu 32. Solid lines are the best global nonlinear least-squares fits to eq 8. Values of χ^2 are (a) 7.77, (b) 5.93, (c) 5.88, and (d) 5.41. Fitted parameters are given in Table 3 and were used to determine the protein folding kinetics and equilibrium constant.

Table 3. Chemical Exchange Parameters for α_2D

residue	R_2^0 (s^{-1})	p_M	$\Delta\omega$ (ppm)	k_{ex} (s^{-1})
Leu 6	22.6 ± 0.5	0.038 ± 0.006	0.89 ± 0.11	510 ± 170
Leu 13	22.6 ± 0.4	0.028 ± 0.007	1.12 ± 0.15	580 ± 220
Leu 25	25.0 ± 0.6	0.019 ± 0.002	1.31 ± 0.17	940 ± 310
Leu 32	21.7 ± 0.5	0.024 ± 0.004	1.16 ± 0.13	540 ± 160

(monomer) α_2D sample. All $R_2(1/\tau_{cp})$ relaxation rate constants are given in the Supporting Information. Data recorded at either $B_0 = 11.7$ or 14.1 T can be fit adequately to the fast-limit equation describing chemical exchange in CPMG experiments when $k_{ex}/\Delta\omega \gg 1$.[54] However, the fitted values of k_{ex} were not independent of the static field strength, and the amplitude of the relaxation dispersion curves, R_{ex}, did not vary as B_0^2 as expected for fast-limit exchange.[55] Self-consistent results for the kinetic parameters were obtained by global fitting of the relaxation dispersion curves obtained at $B_0 = 11.7$ and 14.1 T with the general form of eq 8. The fitted relaxation dispersion data are shown in Figure 8, and optimized parameters are given in Table 3. For all residues, the chemical exchange process occurs in the slow regime ($k_{ex}/\Delta\omega < 1$) on the chemical shift time scale. The ratios of R_{ex} at $B_0 = 14.1$ T relative to R_{ex} at $B_0 = 11.7$ T range from 1.08 ± 0.10 for Leu 32 to 1.16 ± 0.10 for Leu 25, compared with a factor of 1.44 expected for quadratic scaling. The largest value of $\Delta\omega$ at $B_0 = 14.1$ T is 500 s^{-1} for Leu 25; therefore, conventional CPMG R_2 measurements acquired with $\tau_{cp} = 0.5$ ms satisfy the fast-pulsing criterion, $1.5/\tau_{cp} > \Delta\omega$, and $\Delta R_2(1/\tau_{cp})$ varies as B_0^2 for both slow and fast exchange processes. The quadratic dependence of Γ on B_0 in Figure 2 does not contradict the observation that the field dependence of R_{ex} is less than quadratic. Rather, only the field dependence of the amplitude of R_{ex} is an accurate indicator of the time scale of chemical exchange.[55] The results for Leu 6, Leu 13, and Leu 32 are very similar, while Leu 25 has a substantially larger value of k_{ex} and probably is affected partially by an additional exchange mechanism (vide infra). The average results for $p_M = 0.028 \pm 0.003$ and $k_{ex} = 540 \pm 100$ s^{-1} for Leu 6, Leu 13, and Leu 32 yield estimates of $K_d = 2.7 \pm 0.6$ μM, $k_1 = 15 \pm 3$ s^{-1}, and $k_{-1} = (4.7 \pm 0.9) \times 10^6$ M^{-1} s^{-1}. The value of K_d is in accordance with earlier estimates of $K_d = 7 \pm 3$ μM, determined for a sample in 100% H_2O.[27]

Discussion

The dynamics of the backbone of α_2D on picosecond to nanosecond and microsecond to millisecond time scales were assessed by measuring nuclear magnetic spin relaxation rate constants for the $^{13}C^{\alpha}$ of Leu 6, 13, 25, and 32, together with their symmetry-related counterparts Leu 6′, 13′, 25′, and 32′. These leucine residues are spatially distributed throughout the hydrophobic core of the dimeric structure of α_2D (Figure 2). Backbone dynamics on picosecond to nanosecond time scales were characterized by reduced spectral density mapping and the model-free approach applied to R_1, R_2, and σ_{CH} relaxation rate constants measured at four static magnetic field strengths. The folding kinetics of α_2D were characterized by global analysis of relaxation-compensated CPMG relaxation dispersion measurements at two static magnetic field strengths. In the following, the implications of these results are discussed both for NMR spectroscopy and for protein design and folding.

Reduced spectral density mapping has proven to be a useful approach for interpreting ^{15}N relaxation rate constants, particularly for highly dynamic systems;[29,30] however, relatively few applications have been reported for ^{13}C.[47,48] Reduced spectral density mapping is facilitated for ^{15}N because $\omega_H + \omega_N \approx 0.9\omega_H$ and $\omega_H - \omega_N \approx 1.1\omega_H$ are close to ω_H;[46] in contrast, the frequencies $\omega_H - \omega_C \approx 0.75\omega_H$ and $\omega_H + \omega_C \approx 1.25\omega_H$ differ substantially from ω_H. Consequently, the spectral densities $J(\omega_H - \omega_C)$, $J(\omega_H)$, and $J(\omega_H + \omega_C)$ are more difficult to approximate, particularly using relaxation rate constants acquired at a single magnetic field strength.[48] In the present approach, the dependence of σ_{CH} on B_0^{-2} was measured directly from data acquired at four static magnetic fields, and $J(\beta\omega_H)$ was obtained empirically from a linear least-squares fit to the frequency dependence of σ_{CH}. This method is similar to the first-order Taylor series expansion of $J(\omega)$ proposed by Farrow and coworkers.[46] In addition, the field dependence of Γ illustrated in Figure 5 allows $J(0)$ to be determined from eq 5 even in the presence of chemical exchange affecting all Leu residues. For well-ordered globular proteins, model-free parameters determined from reduced spectral density mapping and direct analysis of relaxation rate constants should yield similar results. As shown in Table 2, results for α_2D obtained by these two methods are indistinguishable, even for the most mobile residue, Leu 32. Numerical simulations also indicate that accurate results for α_2D are obtained from the proposed reduced spectral density mapping approach, provided that intramolecular correlation times are approximately <80 ps or >1 ns. These results demonstrate that reduced spectral density mapping can be applied to ^{13}C spin relaxation data with similar robustness and utility as for ^{15}N, if relaxation rate constants are measured at multiple static magnetic fields.

The present investigation represents the first application of relaxation-compensated CPMG experiments to directly measure the kinetics of a protein folding equilibrium. The use of ^{13}C relaxation for investigations of protein folding has two advantages compared with ^{15}N relaxation.[63] First, exchange of H^N protons with solvent is not a concern. Second, $^{13}C^\alpha$ chemical shifts relative to random coil values are sensitive to secondary structure in proteins.[36,64] Thus, linebroadening resulting from exchange between folded and unfolded species has an easily interpreted physical basis. As exemplified by the present results, accurate assessment of chemical exchange in proteins requires evaluating the static magnetic field strength dependence of exchange linebroadening.[55] Characterization of kinetic rate constants for folding using $R_{1\rho}$ and CPMG measurements of chemical exchange should be applicable broadly to systems in which the unfolded states have populations ≥ 0.02.[63]

By design, α_2D is a symmetric, homodimeric four-helix bundle. Equilibrium thermal denaturation experiments in H_2O demonstrate that α_2D unfolds in a cooperative two-state transition between folded dimers and unfolded monomers.[27] The folding rate constant, $k_{-1} = (4.7 \pm 0.9) \times 10^6\ M^{-1}\ s^{-1}$, measured for α_2D is consistent with the rate constants measured for other small helical dimeric proteins. P22 Arc repressor, a 106-residue dimeric protein that contains a helical bisecting U structural motif similar to that of α_2D, folds with a rate constant of $1 \times 10^7\ M^{-1}\ s^{-1}$.[65] A variant of GCN4p1, a 33-residue dimeric coiled coil with a $\Delta G°$ of folding similar to that of α_2D, folds with a rate constant of $2 \times 10^6\ M^{-1}\ s^{-1}$.[66] These folding on-rates are approximately 3 orders of magnitude slower than the diffusion-limited rates estimated for proteins of this size.[65] The rate reductions most likely reflect the necessary formation of specific polar interactions that are crucial to the folds of these proteins. This hypothesis is supported by the observation that the folding rate constants increase by 2 orders of magnitude for variants of Arc and GCN4 that have reduced electrostatic interactions.[67,68] The unfolding off-rate for α_2D, $k_1 = 15 \pm 3\ s^{-1}$, is about 2 orders of magnitude larger than that for Arc, $k_1 = 0.1\ s^{-1}$. This difference most likely reflects the smaller hydrophobic core of α_2D (70 residues) compared with that of Arc (106 residues).[65]

The changes in $^{13}C^\alpha$ chemical shift values between unfolded and folded α_2D, $\Delta\omega$, obtained from the analysis of the chemical exchange folding kinetics (~1 ppm) are less than the predicted change in $^{13}C^\alpha$ chemical shifts relative to random coil (~2 ppm). Therefore, the ensemble of unfolded states involved in the exchange process at equilibrium may include transiently populated, partially structured helical conformations rather than the fully unfolded random coil observed in high concentrations of denaturant.[69] This observation is consistent with earlier studies showing that the thermally unfolded state of α_2D retains significant secondary structure, as inferred from CD spectroscopy.[27] Studies of a precursor of α_2D led to the proposal that a successfully designed dimeric helical protein would populate some partially helical conformations in the unfolded monomeric state.[70] If the representation of helical states in the monomeric ensemble is too low, then the energetic costs are too great for successful folding, whereas too large a population of helical conformations is antithetical to cooperative folding. The present results, derived from chemical exchange measurements, corroborate this hypothesis and suggest that the native-like properties of the α_2D dimer result in part from the appropriate degree of inherent helical content in the equilibrium unfolded ensemble. More recently, our design strategy has emphasized the three states of a polypeptide—native, compact intermediate, and unfolded—that must be considered in an optimal de novo approach.[2,71] These considerations also have been shown to be important for natural proteins.[72,73]

The mobility of the backbone of α_2D on picosecond to nanonsecond and microsecond to millisecond time scales is typical of natural proteins. All of the leucine $^{13}C^\alpha$ spins have high order parameters, S^2, reflecting a high degree of motional restriction on the picosecond to nanosecond time scale. Leucines 13 and 25 are slightly more ordered ($S^2 = 0.95 \pm 0.01$ and 0.96 ± 0.01, respectively) than Leu 6 and Leu 32 ($S^2 = 0.92 \pm 0.01$ and 0.87 ± 0.04, respectively); in addition, internal correlation times are sufficiently large to contribute significantly to the spectral density functions for Leu 6 and 32. The nominal increase in mobility of the backbone C^α of Leu 6 and 32 also is reflected in the ensemble of low-energy NMR structures[23] and is most likely due to a slight fraying of the N-terminus of helix 1 and the C-terminus of helix 2. Residues Leu 6, Leu 13, and Leu 32 appear to be highly ordered on the microsecond to millisecond time scale because exchange linebroadening of the $^{13}C^\alpha$ resonances is explained completely by the folding equilibrium. Only Leu 25 exhibits evidence for intramolecular conformational heterogeneity within the folded dimer state on the microsecond to millisecond time scale. Evidence for additional exchange contributions for Leu 25 is provided by both the larger slope observed for Leu 25 in Figure 5 and the different values of k_{ex} and R_2^0 reported in Table 3 compared with those of the other residues. Leu 25 and Leu 13 have nearly identical $J(0)$ values; therefore, the larger value of R_2^0 for Leu 25 suggests that an exchange process occurs on a time scale faster than the largest value of $1/\tau_{cp}$ utilized in the present experiments (2000 s^{-1}). Examination of a superposition of the family of NMR structures indicates that the Leu 25 side chain populates two distinct χ_2 rotomers. Thus, additional exchange contributions for Leu 25 may arise from interconversion between these two conformations. The characterization of dynamic properties on picosecond to nanosecond and microsecond to millisecond time scales corroborates and extends our previous findings indicating that α_2D is a native-like protein.[23]

---

[63] Vugmeyster, L.; Kroenke, C. D.; Picart, F.; Palmer, A. G.; Raleigh, D. P. *J. Am. Chem. Soc.* **2000**, *122*, 5387−5388.

[64] Wishart, D. S.; Sykes, B. D. *Methods Enzymol.* **1994**, *239*, 363−392.

[65] Milla, M.; Sauer, R. *Biochemistry* **1994**, *33*, 1125−1133.

[66] Sosnick, T. R.; Jackson, S.; Wilk, R. R.; Englander, S. W.; DeGrado, W. F. *Proteins: Struct., Funct. Genet.* **1996**, *24*, 427−432.

[67] Waldburger, C.; Jonsson, T.; Sauer, R. *Proc. Natl. Acad. Sci. U.S.A.* **1996**, *93*, 2629−2634.

[68] Durr, E.; Jelesarov, I.; Bosshard, H. *Biochemistry* **1999**, *38*, 870−880.

[69] Shortle, D. *FASEB J.* **1996**, *10*, 27−34.

[70] Ho, S. P.; DeGrado, W. F. *J. Am. Chem. Soc.* **1987**, *109*, 6751−6758.

[71] Hill, R. B.; DeGrado, W. F. *Struct. Folding Des.* **2000**, *8*, 471−479.

[72] Munoz, V.; Cronet, P.; Lopez-Hernandez, E.; Serrano, L. *Folding Des.* **1996**, *1*, 167−178.

[73] Viguera, A.; Villegas, V.; Aviles, F.; Serrano, L. *Folding Des.* **1997**, *2*, 23−33.

The backbone motions of α_2D are interesting in light of the forces that govern the native-like behavior of this protein. The strategy for the design focused on generating a well-packed hydrophobic core and specifying interactions at each of the four helical interfaces found in a four-helix bundle.[27] At one interface (helix 1/1′), hydrophobic interactions between leucines provide the primary driving force for folding.[23] In contrast, the helix 2/2′ interface is formed by a hydrogen-bonding network that is essential for native-like behavior.[28] The effects of these different protein folding forces on backbone mobility within the folded state can be compared using the data presented herein. The order parameters clearly show that helix 1 and helix 2 exhibit the same degree of motional restriction, despite the fundamental differences between the forces that drive their folding. Thus, α_2D exhibits both hydrophobic and hydrogen-bonding forces that result in motional behavior similar to that found in natural proteins.

Conclusion

NMR spin relaxation methods have been used to characterize intramolecular dynamical and folding kinetic properties of α_2D, a de novo designed dimeric four-helix bundle labeled with ^{13}C at the C$^{\alpha}$ position of eight leucine residues spatially distributed throughout the protein. This study is the starting point for a thorough investigation of the relationship between molecular motion, protein folding, and structure. The results reported for the Leu ^{13}C$^{\alpha}$ spins both confirm the success of the overall design strategy and suggest avenues for further improvement of the native-like properties of α_2D. Elucidation of the backbone dynamics of α_2D is a necessary first step prior to conducting side-chain NMR spin relaxation experiments that will probe mobility within the hydrophobic core of α_2D. These studies, in progress, promise to provide additional insights into protein mobility and structure. The experimental approaches for characterizing protein dynamics using ^{13}C reduced spectral density mapping and for characterizing protein folding kinetics using ^{13}C chemical exchange linebroadening that have been have been applied to α_2D can be extended to other macromolecular systems. These techniques will contribute to improved understanding of conformational dynamics and folding in proteins and other biological macromolecules.

Acknowledgment. We thank Kathleen P. Howard (Swarthmore College) for access to the Bruker DRX400 NMR spectrometer, Peter J. Domaille (Dupont Pharmaceutical) for access to the Bruker AMX600 MHz NMR spectrometer, and the National Magnetic Resonance Facility at Madison (NMRFAM) for access to the Bruker DRX750 MHz NMR spectrometer. We also thank Brian F. Volkman (NMRFAM) for assistance with NMR spectroscopy. NMRFAM is supported by the NIH Biomedical Technology Program (RR02301), with additional equipment funding from the University of Wisconsin, NSF Academic Infrastructure Program (BIR-9214394), NIH Shared Instrumentation Program (RR02781, RR08438), NSF Biological Instrumentation Program (DMB-8415048), and U.S. Department of Agriculture. R.B.H. and C.B. acknowledge support from National Research Service Awards GM18491 and GM17562, respectively. This work was supported by National Institutes of Health Grants GM54616 (W.F.D.) and GM59273 (A.G.P.) All in-house software programs are available from http://cpmcnet.columbia.edu/dept/gsas/biochem/labs/palmer.

Supporting Information Available: Four tables containing R_1, R_2, and σ_{CH} values for α_2D measured at $B_0 = 9.4$, 11.7, 14.1, and 17.6 T, and two tables containing $R_2(1/\tau_{cp})$ values for α_2D measured at $B_0 = 11.7$ and 14.1 T (PDF). This material is available free of charge via the Internet at http://pubs.acs.org.

JA001129B